Scaling of Impulsively Started, Incompressible, Laminar Round Jets and Pipe Flows

Tang-Wei Kuo*
General Motors Technical Center, Warren, Michigan
Saadat A. Syed*
United Technologies Corporation, Pratt & Whitney Group, East Hartford, Connecticut
and
Frediano V. Bracco†
Princeton University, Princeton, New Jersey

The scaling law of transient and steady, laminar, incompressible round jets is deduced from numerical solutions of the complete Navier-Stokes equations for $70 \le Re \le 500$, and the results are compared with available experimental data. It is found that the axial length scale is DRe and the time scale D^2/ν. The same scales are shown to apply also to the entrance and fully developed regions of transient and steady pipe flows for $Re > 10$.

Nomenclature

D = orifice, or pipe, diameter
L = axial extent of the computation domain
p = static pressure
r = radial coordinate
R = radial extent of computation domain
Re = $\bar{U}D/\nu$ Reynolds number
t = time, or jet arrival time
T_s = steadying time for transient pipe flows
u = axial component of the velocity
$u_{\ell,x}$ = centerline value of u at x
$\bar{U}$ = cross-section average of the jet, or pipe, velocity
v = radial component of the velocity
x = axial coordinate
X_v = axial distance of the virtual origin
μ = viscosity
ν = kinematic viscosity
ρ = density

Introduction

THE transient of laminar jets does not seem to have been extensively investigated. Abramovich and Solan[1] presented experimental and theoretical results for the speed of travel of the spherical vortex at the front of incompressible, impulsively started, submerged laminar jets. They found that, for a given exit velocity profile, the time t required for the centerline velocity of the jet to reach 70% of its steady-state value at any axial location x is a function of the diameter of the orifice D, the mean exit velocity $\bar{U}$, and the kinematic viscosity ν. They proposed for the characteristic axial length and time scales $DRe^{1/2}$ and $DRe^{1/2}/\bar{U}$, where $Re = \bar{U}D/\nu$. By solving numerically the complete Navier-Stokes equations, we show that the actual scales are DRe and $DRe/\bar{U}$ and that the same scales apply also to incompressible, impulsively started, laminar pipe flows for $Re > 10$.

Received Aug. 23, 1984; revision submitted July 17, 1985.

*Research Engineer.

†Professor, Mechanical Engineering. Member AIAA.

Transient Jets

Equations and Method of Solution

The governing equations and boundary conditions are:

$$\frac{\partial u}{\partial x} + \frac{1}{r}\frac{\partial (rv)}{\partial r} = 0 \tag{1}$$

$$\frac{\partial u}{\partial t} + u\frac{\partial u}{\partial x} + v\frac{\partial u}{\partial r} = -\frac{1}{\rho}\frac{\partial p}{\partial x} + \nu\left[\frac{\partial^2 u}{\partial x^2} + \frac{1}{r}\frac{\partial}{\partial r}r\frac{\partial u}{\partial r}\right] \tag{2}$$

$$\frac{\partial v}{\partial t} + u\frac{\partial v}{\partial x} + v\frac{\partial v}{\partial r} = -\frac{1}{\rho}\frac{\partial p}{\partial r} + \nu\left[\frac{\partial}{\partial r}\frac{1}{r}\frac{\partial (rv)}{\partial r} + \frac{\partial^2 v}{\partial x^2}\right] \tag{3}$$

$$\left.\begin{aligned} &\text{at } r=0, \quad \frac{\partial u}{\partial r}=0, \quad v=0 \\ &\text{at } r=R, \quad u=0, \quad \frac{\partial (rv)}{\partial r}=0 \\ &\text{at } x=0, \quad u=U(0,r) \text{ for } r\le D/2 \\ &\qquad\qquad u=0 \qquad\quad \text{for } r>D/2 \end{aligned}\right\} \tag{4}$$

where R and L are the radial and axial dimensions of the integration domain, respectively, and the other symbols have their standard meanings. The initial conditions are zero velocity everywhere except at the nozzle exit, where the radial profile is specified.

If the boundary-layer approximation is made, $\partial^2 u/\partial x^2 = \partial^2 v/\partial x^2 = \partial p/\partial x = \partial p/\partial r = 0$, and if the following dimensionless parameters are introduced:

$$\left.\begin{aligned} &u^* = u/\bar{U}, \qquad v^* = Rev/\bar{U}, \qquad U^* = U/\bar{U} \\ &x^* = x/DRe, \qquad r^* = r/D, \qquad t^* = t/(DRe/\bar{U}) \end{aligned}\right\} \tag{5}$$

then the remaining terms in Eqs. (1-4) become Reynolds number-independent. Thus, under the boundary-layer approximation, the axial length and time scales are DRe and $DRe/\bar{U}=D^2/\nu$.

The complete equations were then solved numerically to check the boundary-layer scales and to compare our results with available experimental data. Theoretically, the velocity goes to zero only as r tends to infinity. Conditions (4) are for an axisymmetric field and a finite domain of integration. Our practice has been to choose R approximately equal to 3.5 times the maximum half-jet half-radius at the jet outlet plane and to compute the axial velocity at $x=L$ by integral mass balance.

An expanding grid was used with an axial expansion factor of 5% and a radial one of 7%, except within the pipe exit where the grid was uniform. Generally, 32 radial and 42 axial cells were employed. The complete set of Eqs. (1-4) were solved by an iterative finite difference technique that employs a hybrid difference scheme for the convection terms that reduces to the upwind difference when the absolute value of the cell Reynolds number ($u\Delta x/\nu$, $v\Delta r/\nu$) is >2 and to a central difference when ≤ 2. In all steady and transient calculations, the cell Reynolds number in the radial direction was <2. The central differencing made the radial momentum transfer calculation more accurate. In addition, for each case we recorded physical axial diffusion, numerical axial diffusion (based on the upwind difference analysis), and axial convection in each cell. In the mixing-layer region ($x/D>0.5$), the axial convection term was, in general, much larger (two orders of magnitude) than both physical and numerical diffusion, and for both steady and transient cases. The diffusion terms occasionally were as large as 25% of the convection terms but only very near the nozzle exit ($x/D\leq 0.5$) and on account of the large cross flow. The value of the time increment increased during the computations so as to keep the additional jet penetration during each time step approximately constant as the jet slows down. A uniform time-step calculation was also made and gave practically identical results but required three times as much CPU time. Finally, for each flow configuration, grid independence was checked. Typically, an increase in cells from 42×32 to 84×64 resulted in a variation of less than 4% in the centerline velocity and in an increase by a factor of 7 in CPU time.

Results

Computed steady-state centerline velocities and transient jet tip penetration histories, starting from a parabolic exit velocity profile, for $Re=100$, and for three different values of $\bar{U}$, D, ν, are shown in Figs. 1 and 2. The dimensionless coordinates are those suggested by Abramovich and Solan: $x^*=x/DRe^{1/2}$, $t^*=2t\nu Re^{1/2}/D^2$. And the jet arrival time t is defined as by Abramovich and Solan: the time needed for the axial velocity u to reach 70% of its steady-state value at any given axial location. Numerically it is determined as illustrated in Fig. 3, where the time variations of the computed centerline axial velocities at various downstream axial locations are shown and the 70% values indicated. Parenthetically, Fig. 3 also shows the velocity overshoot of the jet head vortex that was measured by Abramovich and Solan and that would not have been computed if only the boundary-layer equations had been solved.

In Figs. 1 and 2, it is observed that the computed solutions for a constant $Re=100$ and different values of $\bar{U}$, D, ν are identical and that the calculated results are at the boundary of, or within, the experimental range. But Figs. 4 and 5 show that the computed steady and transient solutions for different $Re=70$, 100, 500 do not coincide when the nondimensional parameters of Abramovich and Solan are used and continue to show a systematic Reynolds number dependence. Notice, however, that the computed curves for $70\leq Re\leq 500$ bracket the experimental measurements of Abramovich and Solan for $80\leq Re\leq 500$. Thus, we would like to suggest that what Abramovich and Solan considered experimental scatter is actually due to improper account of the Reynolds number in their nondimensional parameters.

Indeed, the numerical solutions of the complete equations coalesce when plotted using the dimensionless parameters x/DRe and $t/(D^2/\nu)$, as shown by the lower curves of Figs. 6 and 7. The same scaling also applies for a uniform exit velocity profile as shown by the upper curves in the same

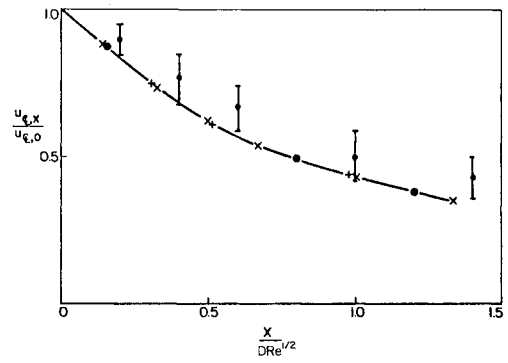

Fig. 1 Computed and measured steady-state centerline velocity at fixed $Re=100$: + computed with $\bar{U}=12$ cm/s, $D=1.2$ cm, $\nu=0.144$ cm^2/s; x computed with $\bar{U}=12$ cm/s, $D=12$ cm, $\nu=1.44$ cm^2/s; • computed with $\bar{U}=1.2$ cm/s, $D=12$ cm, $\nu=0.144$ cm^2/s; ✤ measured[1] with $80\leq Re\leq 500$.

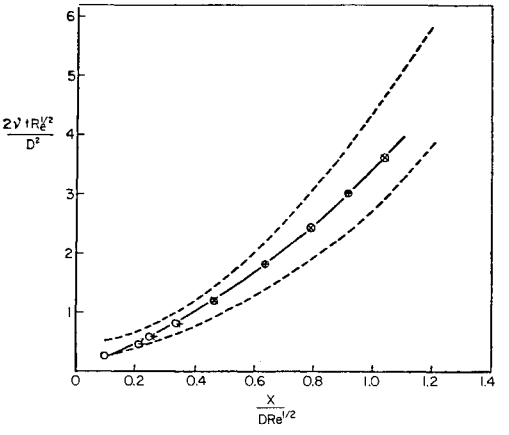

Fig. 2 Computed and measured transient jet tip penetration at fixed $Re=100$: + computed with $\bar{U}=12$ cm/s, $D=1.2$ cm, $\nu=0.144$ cm^2/s; x computed with $\bar{U}=12$ cm/s, $D=12$ cm, $\nu=1.44$ cm^2/s; o computed with $\bar{U}=1.2$ cm/s, $D=12$ cm, $\nu=0.144$ cm^2/s; ---- measured[1] with $80\leq Re\leq 500$.

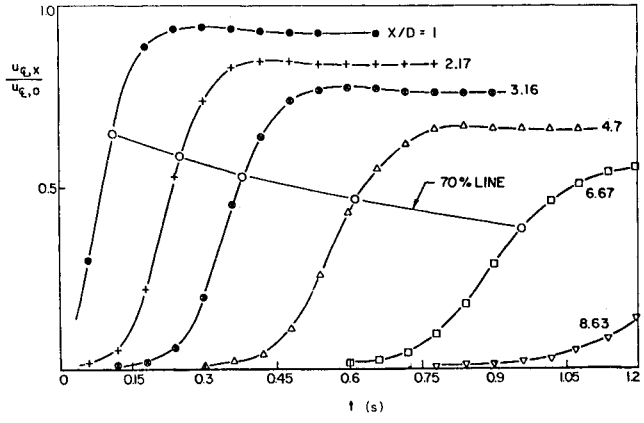

Fig. 3 Definition of transient arrival time at various x/D locations ($\bar{U}=12$ cm/s, $D=1.2$ cm, $\nu=0.144$ cm^2/s, $Re=100$).

figures. Unfortunately, the experimental data of Abramovich and Solan cannot be put in Fig. 7 because they give insufficient information to identify the Reynolds number corresponding to each of their experimental points. However, in Fig. 6, measured and computed data by du Plessis et al.,[2] Andrade and Tsien,[3] Pai and Hsieh,[4] and Hatta and Nozaki[5] are also given and seem to agree with our results.

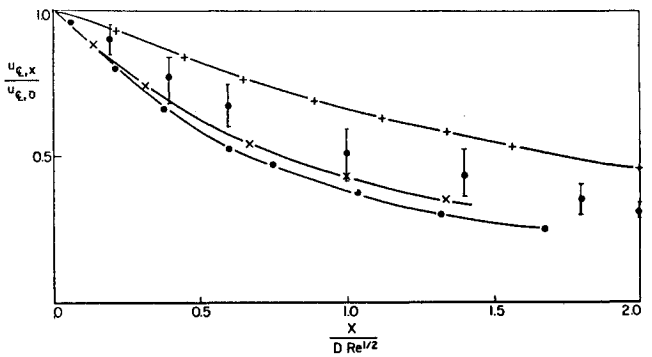

Fig. 4 Computed and measured steady-state centerline velocity for different *Re* using the length scale $DRe^{1/2}$: • computed with $Re=70$; *x* computed with $Re=100$; + computed with $Re=500$; ✦ measured[1] with $80 \leq Re \leq 500$.

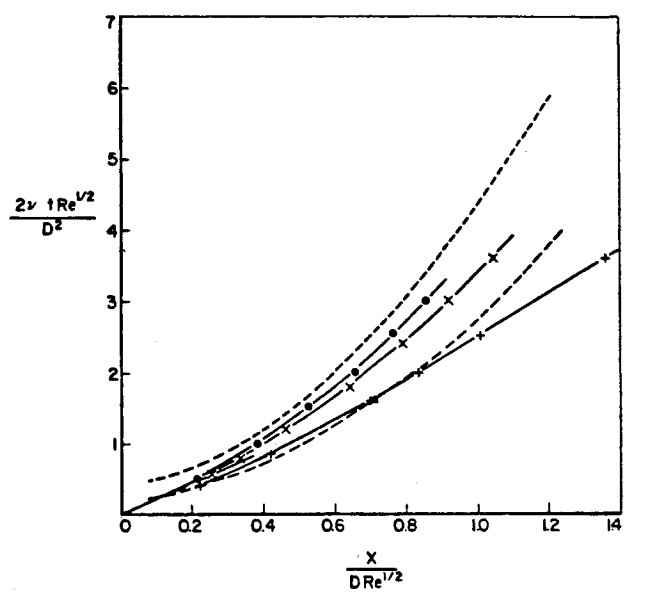

Fig. 5 Computed and measured transient jet tip penetration for different *Re* using the length scale $DRe^{1/2}$ and the time scale $D^2/2\nu Re^{1/2}$: • computed with $Re=70$; *x* computed with $Re=100$; + computed with $Re=500$; ---- measured[1] with $80 \leq Re \leq 500$.

Thus, the scaling suggested by the boundary-layer approximation is confirmed by the numerical solutions of the complete equations and the available experimental data.

For a given initial velocity profile, the universal curve of Fig. 7 changes if a different definition is adopted to identify the arrival of the jet, but the characteristic time and length scales remain the same. This is illustrated in Fig. 8 for the case of uniform exit velocity, where the 70% $u_{\ell,\text{steady}}$ curve is shown together with the 99.9% $u_{\ell,\text{steady}}$ and 99.9% steady momentum curves. The latter is obtained by considering the time at which the axial momentum reaches 99.9% of its steady value at each axial location.

Virtual Origin

Since the numerical solutions of the complete equations scale as predicted with the simplified boundary-layer equations, use of Schlichting's point source model[6] is justified. After introducing the kinematic momentum, based on the jet exit velocity profile, his solution can be rearranged to give the following centerline velocity decay equations for uniform and parabolic exit velocity profiles:

$$(u_{\ell,x}/u_{\ell,0})(x/DRe) = 3/32 \text{ (uniform)} \tag{6}$$

$$(u_{\ell,x}/u_{\ell,0})(x/DRe) = 2/32 \text{ (parabolic)} \tag{7}$$

By plotting the above two curves along with the computed results of Fig. 6, the following two expressions for the locations of the two virtual origins are found simply by shifting corresponding curves horizontally (see Fig. 9):

$$X_v = .07DRe \text{ (uniform)} \tag{8}$$

$$X_v = .05DRe \text{ (parabolic)} \tag{9}$$

The boundary conditions used in our computations, Eqs. (4), are for wall jets with slip at the wall. For submerged jets and uniform profile, Rankin and Sridhar[7] found $X_v = .064DRe$ from their analysis and Greene[8] found $X_v = .07DRe$ from his experiments. For submerged jets and parabolic profile, du Plessis et al.[2] found experimentally $X_v = .055\ DRe$. For wall jets, the constants in Eqs. (8) and (9) can be expected to be smaller since the initial axial entrainment near the nozzle exit is reduced. This is the trend indicated by the results of Andrade and Tsien[3] for both parabolic ($X_v = .04DRe$ measured) and uniform ($X_v = .056DRe$ computed) exit velocity profiles.

Transient Pipe Flows

Equations and Method of Solution

The equations and boundary conditions for the pipe flow are the same as for the jet except for the no-slip condition at the pipe wall, i.e., at $r=R=D/2$, $u=v=0$. Method of solution and numerical considerations are also the same except for a uniform grid of 42 axial and 32 radial cells and for the

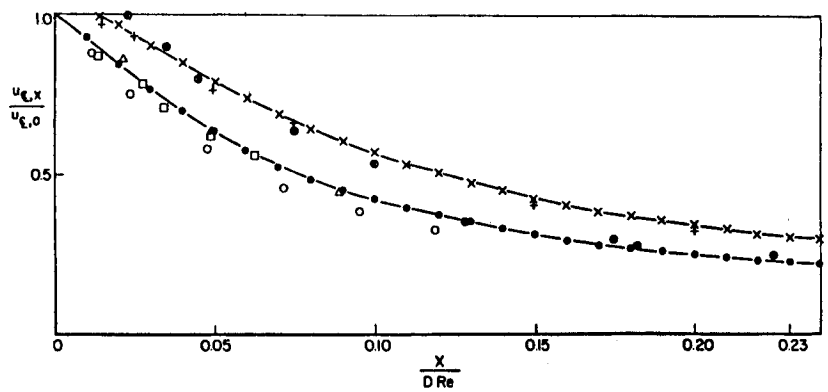

Fig. 6 Computed and measured steady-state centerline velocity using the length scale *DRe*. Parabolic exit velocity profile: • computed with $Re=70,100,500$; 0 measured[2] with $Re=168$; □ measured[2] with $Re=290$; △ measured[3] with $Re=400$; ✦ measured[3] with $100 \leq Re \leq 600$. Uniform exit velocity profile: *x* computed with $Re=100, 200, 500$; + computed[4]; ✦ computed.[5]

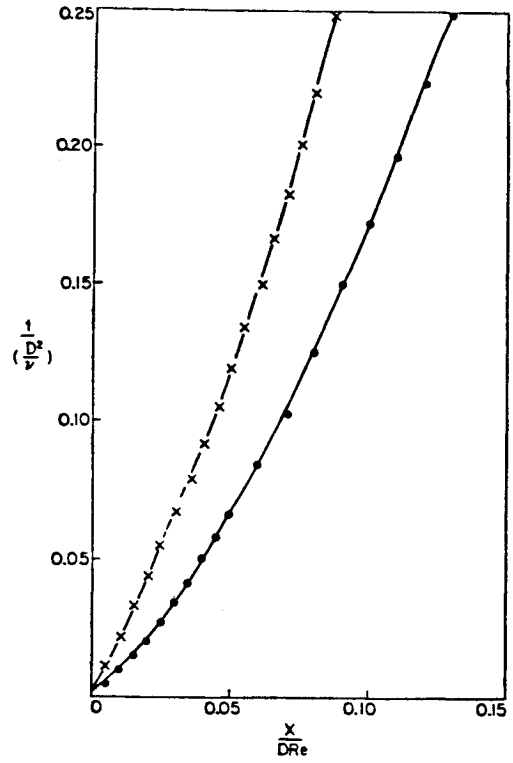

Fig. 7 Computed transient jet tip penetration using the length scale DRe and the time scale D^2/ν: • parabolic exit velocity profile for $Re=70$, 100, 500; x uniform exit velocity profile for $Re=100$, 200, 500.

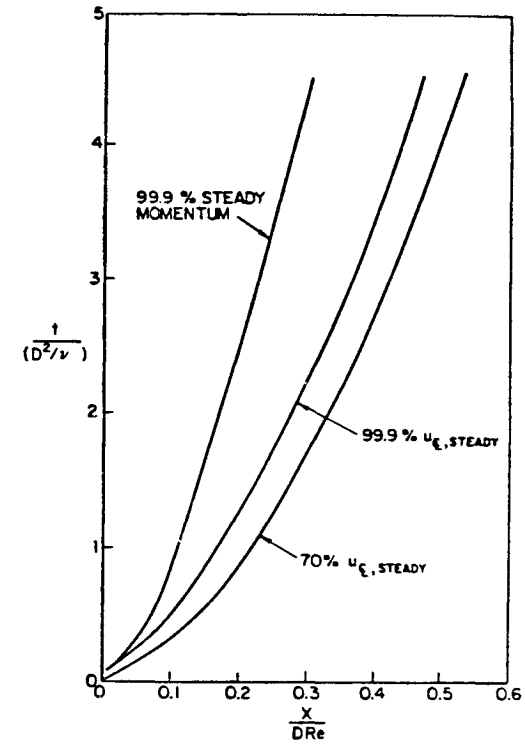

Fig. 8 Computed transient jet tip penetration using different definitions for the tip.

cell Reynolds number having always been <2. Computations with 84×64 cells yielded smaller than 1% change in the dependent variables and required more than one order of magnitude greater CPU time.

Results

Szymanski[9] obtained an analytical solution for the transient of the laminar pipe flow in the fully developed region by assuming that $v=0$, $u=u(r,t)$ and by using a constant pressure gradient. He showed that the characteristic time is D^2/ν. In the entrance region the simplified boundary-layer equations can still be considered and independence of Re obtained if DRe and $DRe/\bar{U}=D^2/\nu$ are selected as the axial length and time scales. These two limit cases suggest that the axial scales of pipe flows are the same as those of jets. The conclusion is confirmed by the numerical solution of the complete equations.

The steadying time T_s, evaluated at various cross sections in the entrance region, is defined as the time from the start of the flow to the point at which the time derivative in the axial momentum equation becomes less than 0.5% of any of the other terms. The maximum steadying time $T_{s\,max}$ is defined as the time needed to meet the same criterion in the fully developed parabolic velocity profile region. In order to ensure that a fully developed velocity profile is obtained, the calculation domain was specified so that it was greater than the entrance length for each Reynolds number studied.

Solutions of the complete Navier-Stokes equations were obtained first for $Re=100$ and three different combinations of the values of $\bar{U}$, D, ν. The results, presented in Fig. 10, show that T_s tends to $.05D^2/\nu$ for sufficiently large x, i.e., $T_{s\,max}=.05D^2/\nu$, and also that the ratio $T_s/T_{s\,max}$ vs the dimensionless distance x/DRe is the same for all three combinations. The approximate analytical solution of Szymanski for the fully developed region also yields the proportionality of the steadying time to the diffusion time, but Szymanski's proportionality constant is 0.12 (obtained by requiring the centerline velocity to reach 95% of its steady-state value) in-

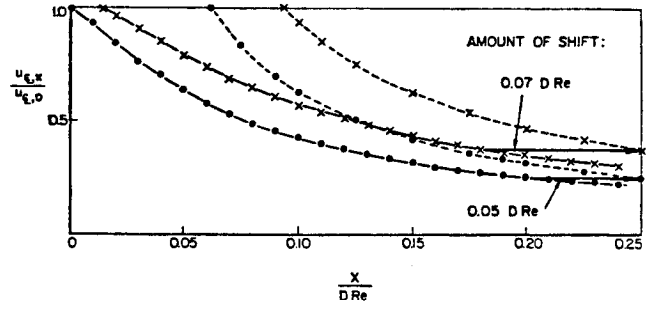

Fig. 9 Graphic determination of the location of the virtual origin, X_v, using the computed steady-state centerline velocity. Parabolic exit velocity profile: —•— computed; --•-- analytical solution,[6] Eq. (6). Uniform exit velocity profile: —×— computed; --×-- analytical solution,[6] Eq. (7).

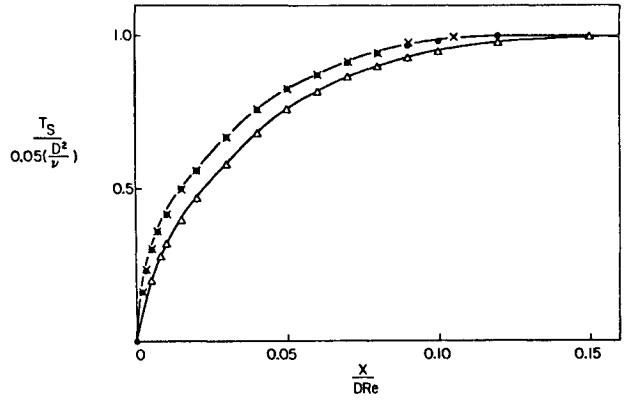

Fig. 10 Computed nondimensional steadying time vs nondimensional distance from the pipe entrance for different Re: Δ $Re=10$; • $Re=100$ (obtained with $\bar{U}=1.13$ cm/s, $D=1.0$ cm, $\nu=1.13\ 10^{-2}$ cm^2/s; $\bar{U}=1.13$ cm/s, $D=0.1$ cm; $\nu=1.13\ 10^{-3}$ cm^2/s; $\bar{U}=0.113$ cm/s, $D=1.0$ cm, $\nu=1.13\ 10^{-3}$ cm^2/s); $xRe=1000$.

stead of .05 (with our definition of steadying time, the centerline velocity has reached 99.99% of its steady-state value). The difference in the two constants is not surprising since Szymanski's solution is not of the complete equations and pertains to a slug of fluid in the fully developed region impulsively started under a constant axial pressure gradient whereas in the computations the entrance region is included and a nonuniform and unsteady axial pressure gradient is computed.

The same $T_{s\,\max}$ was also computed with $Re = 10$, 100, 1000, also shown in Fig. 10, thus confirming that the diffusion time is the only characteristic steadying time in this problem. The same figure also demonstrates that, at sufficiently large Re, the only scaling length is DRe. But for very low Re, the entrance length is not directly proportional to Re.

Thus, our results are in general agreement with those already available for limiting cases and show that D^2/ν and DRe are the characteristic time and length scales, respectively, for the transient of incompressible pipe flows, including the entrance region, for $Re > 10$.

Concluding Remarks

Through numerical solutions of the complete Navier-Stokes equations, it has been demonstrated that for impulsively started and steady, laminar, incompressible round jets and for the entrance and fully developed regions of impulsively started and steady, laminar, incompressible pipe flows, the axial length scale is DRe and the time scale is D^2/ν, provided $Re \gg 10$. The corresponding radial length scale is D and axial and radial velocity scales are $\bar{U}$ and $\bar{U}/Re$, respectively, as indicated by Eq. (5). For such flows, pressure gradients and axial diffusion are negligible with respect to convection and radial diffusion.

To illustrate the physical implications of these results, a specific application can be considered. It is desired to determine how long it takes for an impulsively started jet to reach steady state at a given distance from the injector. Given are D, ν, $\bar{U}$, and that the exit velocity profile is uniform. Since diffusion is involved, the precise answer is that steady state is achieved only as time tends to infinity. Practically, one can select a specific fraction of some steady-state quantity and consider steady state to have been reached when that fraction is achieved.

Figure 8 gives three possible definitions. In one case, steady state is reached when the centerline axial velocity achieves 70% of its steady-state value. In the second case, 99.9% of the steady-state centerline velocity is selected and, in the third, 99.9% of the injection momentum. Other definitions could be adopted and more curves would appear in Fig. 8. Whatever the definition, the corresponding curve uniquely relates the dimensionless steady time $t/(D^2/\nu)$ to the dimensionless axial distance $x/(DRe)$. So that, given D, ν, $\bar{U}$, and x, the time to reach steady state can be evaluated. Conversely, jets that have the same values of D^2/ν and DRe would reach steady state at the same distance at the same time. The same exercise could have been done for pipe flows using Fig. 10. But the important point is that DRe and D^2/ν are, respectively, the axial length scale and the time scale for these two families of flows.

Acknowledgments

This work was presented at the 9th DISC Meeting, Princeton University, Princeton, New Jersey, March 1979, and at the 1st FIAT Combustion Workshop, FIAT Research Center, Orbassano, Italy, June 1979. It was supported by the Department of Energy under Contract EC-77-S-02-4192. A002.

References

[1]Abramovich, S. and Solan, A., "The Initial Development of a Submerged Round Jet," *Journal of Fluid Mechanics*, Vol. 59, March 1973, pp. 791-801.

[2]du Plessis, M. P., Wang, R. L., and Tsang, S., "Development of a Submerged Round Laminar Jet from an Initially Parabolic Profile," *Transactions of the ASME, Journal of Dynamic Systems, Measurement, and Control*, Vol. 95, June 1973, pp. 148-154.

[3]Andrade, E. N. and Tsien, H. S., "The Velocity Distribution in a Liquid into Liquid Jet," *Proceedings of the Physical Society, London*, Vol. 49, 1937, p. 381.

[4]Pai, S. I. and Hsieh, T., "Numerical Solution of Laminar Jet Mixing with and without the Free Stream," *Applied Scientific Research*, Vol. 27, 1972, p. 39.

[5]Hatta, K. and Nozaki, T., "Two Dimensional and Axisymmetric Jet Flows with Finite Initial Cross Sections," *Bulletin of the JSME*, Vol. 18, No. 118, April 1975, pp. 349-357.

[6]Schlichting, H., *Boundary Layer Theory*, 6th ed., McGraw-Hill Book Co., New York, 1968.

[7]Rankin, G. W. and Sridhar, K., "Developing Region of Laminar Jets with Uniform Exit Velocity Profiles," *Transactions of the ASME, Journal of Fluids Engineering*, Vol. 100, March 1978, pp. 55-59.

[8]Greene, G. C., "An Investigation of a Free Jet at Low Reynolds Number," M.E. Thesis, Mechanical Engineering Dept., Old Dominion University, Norfolk, VA, 1973.

[9]Szymanski, F., "Quelques solutions exactes des équations de l'hydrodynamique de fluide visqueux dans le cas d'un tube cylindrique," *Journal de Mathématiques Pures et Appliquées*, Series 9, Vol. 11, 1930, p. 67.